Oncology
and Radiotherapy©
20(4) 2026 : 001-009 • RESEARCH ARTICLE

# Radiological Characterization of a Tissue-Equivalent Material for Trabecular Bone: From Diagnostic Imaging to Radiotherapy

**Walid Allioui[123]*, Abdellah khallouqi[1], Hamza Sekkat[1], A. Slimani[1], Abdellah halimi[1], Omar El rhazouani[1]**

[1]Laboratory of Health Sciences and Technologies, Higher Institute of Health Sciences, Hassan 1st University, Settat, Morocco
[2]Higher Institute of Nursing Professions and Health Techniques (ISPITS), Ministry of Health and Social Protection, Marrakech, Morocco
[3]Dar Seha Center of Radiology and Medical Imaging, Marrakech, Morocco

**ABSTRACT**

The development of accurate trabecular bone-equivalent materials remains essential for improving the reliability of anthropomorphic phantoms used in medical imaging and radiotherapy. In this work, an epoxy–$TiO_2$ composite (75/25%) was developed and characterized over a wide photon energy range extending from 10 keV to 25 MeV. The evaluation combined theoretical calculations using the XCOM database, determination of effective atomic number and effective electron density using Phy-X/PSD, and experimental validation through computed tomography.

At low energies (< 40 keV), the mass attenuation coefficient (μ/ρ) shows relative differences ranging from **8% to 14%**, while Z_eff values remain close, with deviations within **±3% to ±5%** around 10 keV. In the diagnostic energy range (50–200 keV), μ/ρ values exhibit a strong agreement, with deviations generally below **2%**, despite larger differences in Z_eff exceeding **20%**. In this same range, N_eff values converge, with relative differences typically within **1% to 3%**, supporting the similarity of photon interaction properties. At higher energies (> 200 keV), including the radiotherapy domain, μ/ρ values remain consistent within **1% to 4%**, indicating stable attenuation behavior across extended energy conditions. Experimental CT measurements yielded Hounsfield Unit (HU) values between **226.9 and 296.8 HU**, with an average of **271.2 HU**, closely matching the clinical reference for trabecular bone (**265.4 ± 3.2 HU**). These results demonstrate that the developed composite provides a reliable approximation of trabecular bone and represents a cost-effective solution for applications in both CT imaging and radiotherapy dosimetry.

**Keywords:** Trabecular bone; Mass attenuation coefficient; Effective atomic number; Effective electron density; Computed tomography; Radiotherapy

**Address for correspondence:**
Walid Allioui
Laboratory of Health Sciences and Technologies, Higher Institute of Health Sciences, Hassan 1st University, Settat, Morocco
E-mail: w.allioui@uhp.ac.ma

**Word count:** 4062 **Figures:** 04 **Table:** 02 **References:** 45

**Received:** 01 April, 2026, Manuscript No. OAR-26-189383;
**Editor assigned:** 04 April, 2026, PreQC No. OAR-26-189383 (PQ);
**Reviewed:** 21 April, 2026, QC No. OAR-26-189383;
**Revised:** 27 April, 2026, Manuscript No. OAR-26-189383 (R);
**Published:** 30 April, 2026

## INTRODUCTION

The use of ionizing radiation in radiotherapy is a cornerstone of modern cancer treatment, where the accurate delivery of dose to target volumes while preserving surrounding healthy tissues is essential [1]. This precision relies on a reliable representation of photon transport and energy deposition in biological tissues at megavoltage (MeV) energies [2]. In parallel, ionizing radiation is extensively employed in medical imaging, where kiloelectronvolt (keV) photon beams are used to visualize anatomical structures with high spatial resolution [3]. Although these two domains operate in distinct energy ranges, they are closely interconnected in clinical practice, particularly for treatment planning, image-guided radiotherapy, and dose verification [4–6]. Consequently, there is an increasing need for tissue-equivalent materials capable of accurately reproducing the radiological behavior of biological tissues across both diagnostic and therapeutic energy ranges [7,8].

From a physical perspective, photon–matter interactions are strongly energy-dependent [9,10]. At low energies, typically below 100 keV, attenuation is dominated by the photoelectric effect [11], which is highly sensitive to the effective atomic number (Z_eff) of the material [12]. In the intermediate energy range relevant to medical imaging, Compton scattering becomes the predominant interaction mechanism and depends [13] mainly on the effective electron density (N_eff) [14]. At higher energies, particularly above 1 MeV, pair production contributes increasingly to photon attenuation [15]. Therefore, a material intended to simulate biological tissues over a wide energy spectrum must reproduce not only its macroscopic density but also its fundamental atomic and electronic properties governing these interaction processes. This requirement represents a significant challenge in the development of versatile and reliable tissue-equivalent materials.

Anthropomorphic phantoms are used in medical physics to simulate human anatomy under controlled conditions without exposing patients to radiation [16]. They are useful in quality assurance [17], system calibration [18], dosimetric validation [19], and experimental studies in both imaging and radiotherapy [20,21]. However, most existing phantoms are designed for a specific application and energy range, and their performance may not be consistent when extended to different conditions [22–25]. In particular, materials optimized for imaging applications may not accurately reproduce tissue behavior at therapeutic energies, and vice versa . This limitation highlights the need for new

materials capable of maintaining consistent radiological properties across a broad energy domain.

The challenge is particularly significant for bone tissue, which exhibits complex composition and heterogeneous structure. Bone is generally classified into cortical and trabecular components, each with distinct radiological characteristics [26]. Trabecular bone, which is characterized by a porous structure and lower mineral density, presents significantly lower radiodensity than cortical bone [27]. In clinical imaging, trabecular bone typically exhibits Hounsfield Unit (HU) values that do not exceed approximately **300 HU**. However, most commercially available and experimentally fabricated phantoms intended to represent bone are designed with significantly higher HU values, often exceeding **500 HU [28]**. As a result, these phantoms tend to represent cortical rather than trabecular bone.

This discrepancy has important implications for both experimental and simulation-based studies. The use of materials with higher-than-realistic HU values may lead to an overestimation of photon attenuation and dose deposition, particularly in applications involving low-density bone structures [29,30]. Consequently, studies conducted using such phantoms may not accurately reflect the radiological behavior of trabecular bone under clinical conditions. This limitation underlines the necessity of developing materials specifically designed to reproduce the properties of trabecular bone with improved fidelity.

To address these challenges, the present study focuses on the development and characterization of a novel tissue-equivalent material intended to simulate trabecular bone. The proposed material is designed to reproduce the radiological properties of this tissue across a wide photon energy range, extending from **10 keV to 25 MeV**, thereby ensuring its applicability in both diagnostic imaging and radiotherapy contexts. This dual applicability represents a key objective of the study, as it enables the use of a single material for multiple clinical and research purposes.

The characterization of the developed material is based on a comprehensive evaluation of its radiological parameters. The mass attenuation coefficient (μ/ρ), effective atomic number (Z_eff), and effective electron density (N_eff) are determined as functions of photon energy using a theoretical calculations based on XCOM and Phy-X/PSD platforms. These parameters provide complementary insights into photon interaction mechanisms and are essential for assessing the equivalence between the developed material and biological bone tissue.

The obtained results are systematically compared with reference data for bone derived from established databases ICRP [31], allowing the identification of potential deviations and their dependence on photon energy. By addressing both the keV and MeV energy domains, this study aims to provide a consistent framework for evaluating tissue-equivalent materials and to contribute to the development of more accurate and versatile phantoms.

Ultimately, the proposed approach seeks to overcome the limitations of existing bone phantoms by introducing a material that more accurately reflects the radiological properties of trabecular bone. This advancement is expected to improve the reliability of experimental measurements and simulation studies, particularly in applications where accurate representation of low-density bone structures is required.

# MATERIALS AND METHODS

## Materials Preparation and Composite Fabrication

The bone-equivalent material was developed using a composite consisting of epoxy resin as the matrix and titanium dioxide ($TiO_2$) as the filler. A composition of 75% epoxy resin ($C_{12}H_{25}ClO_5$) and 25% $TiO_2$ was selected to approximate the radiological properties of adult trabecular bone. The components were accurately weighed and mechanically mixed to ensure a homogeneous dispersion of $TiO_2$ particles within the epoxy matrix. The mixture was then allowed to cure at room temperature until complete polymerization was achieved. To limit the presence of entrapped air, the mixture was processed under controlled stirring conditions and allowed to rest prior to polymerization, facilitating the release of air bubbles and improving material uniformity. The composite was then left to cure at room temperature until complete polymerization was achieved.

To assess the reproducibility of the fabrication process, six samples were prepared under identical conditions. The resulting materials exhibited consistent physical properties, with a measured density of approximately 2.0 g/cm³, in agreement with values reported for bone-equivalent materials in the literature.

## Determination of Elemental Weight Fractions

The elemental composition of the developed epoxy–$TiO_2$ composite [Table1], was determined based on the mass fractions of its constituent elements [Table1]. This step is essential for accurate theoretical calculations of radiological parameters, including the mass attenuation coefficient (μ/ρ), effective atomic number (Zeff), and effective electron density (Neff). The weight fraction of each element i was calculated using the general relation:

$$w_i = \frac{n_i A_i}{\sum_j n_j A_j} \quad (1)$$

Where $n_i$ denotes the number of atoms of the i element in the molecular structure and $A_i$ its corresponding atomic weight. The denominator represents the total molecular weight of the compound. For the composite material, the overall elemental composition was obtained by combining the contributions of each constituent (epoxy resin and $TiO_2$) according to their respective weight fractions. This approach ensures an accurate representation of the material in subsequent simulations and theoretical

**Table 1:** Comparative Elemental Analysis of the Developed Composite and ICRP Trabecular Bone

| Elements | H | C | N | O | Na | Mg | P | S | Ca | Cl | Ti |
|---|---|---|---|---|---|---|---|---|---|---|---|
| **Composite** | 0.06 | 0.39 | - | - | - | - | - | - | - | 0.09 | 0.15 |
| **Trabecular bone ICRP** | 0.034 | 0.155 | 0.042 | 0.435 | 0.001 | 0.002 | 0.103 | 0.003 | 0.225 | - | - |

calculations. In order to assess the suitability of the developed material as a bone-equivalent substitute, a comparative analysis was performed using the elemental composition of adult cranial bone as defined in the ICRP reference human tissue data. The elemental weight fractions of the composite were systematically compared to those of the reference cortical bone to evaluate the level of agreement in terms of atomic composition, which directly influences photon interaction processes and radiological behavior.

### Evaluation of Effective Atomic Number (Z_eff) and Effective Electron Density (N_eff)

The effective atomic number (Zeff) and effective electron density (Neff) of the developed composite were evaluated to assess its radiological equivalence to trabecular bone tissue. These parameters are fundamental for characterizing photon–matter interactions, as Zeff predominantly influences the photoelectric effect at low energies [32], while Neff governs Compton scattering in the diagnostic energy range [33].

The calculations were performed using the Phy-X/PSD software [34], which is based on XCOM photon interaction cross-section data and the elemental composition of the material. Zeff was determined as an energy-dependent parameter by combining the contributions of the constituent elements according to their atomic numbers and weight fractions. Similarly, the effective electron density was calculated from the elemental composition, taking into account the number of electrons per unit mass. The obtained Zeff and Neff values were compared with those of reference trabecular bone derived from ICRP data. This comparison allowed for the evaluation of the material's ability to reproduce the radiological behavior of bone tissue across the investigated energy range, thereby providing additional validation beyond the mass attenuation coefficient (μ/ρ).

### Determination of Mass Attenuation Coefficient (μ/ρ) Using XCOM:

The mass attenuation coefficient (μ/ρ) of the investigated materials was determined using theoretical calculations based on their elemental composition and corresponding mass fractions. The calculations were performed using the XCOM database [35], which provides photon interaction cross-sections over a wide energy range and is commonly used for the evaluation of attenuation properties.

The determination of μ/ρ relies on the Beer–Lambert law, which describes the exponential attenuation of a photon beam as it propagates through a material:

$$I = I_0 e^{-\mu t} \quad (2)$$

Where I0and I represent the incident and transmitted photon intensities, respectively, μ is the linear attenuation coefficient, and t is the material thickness. The mass attenuation coefficient (μ/ρ) was subsequently obtained by normalizing the linear attenuation coefficient to the material density.

The μ/ρ values were calculated over the investigated energy range using XCOM, based on the defined elemental composition. These results were used to analyze the attenuation behavior of the material and to assess its suitability as a bone-equivalent substitute across different photon energies.

### CT Imaging Acquisition and Quantitative Hounsfield Unit (HU) Analysis

Computed tomography (CT) imaging was performed to evaluate the radiodensity of the developed bone-equivalent composite using a clinical Philips Access CT 16 scanner under standardized conditions. Six samples were scanned under identical acquisition parameters, including a tube voltage of 120 kVp, a slice thickness of 1.25 mm, and a rotation time of 0.75 s, consistent with routine adult imaging protocols. For each sample, **three repeated acquisitions** were performed to assess measurement reproducibility. Regions of interest (ROIs) were defined within homogeneous areas of each sample, avoiding edges and air–material interfaces to minimize partial volume effects. The results were expressed as mean ± standard deviation, and the **coefficient of variation (CV %)** was calculated to quantify the dispersion of the measurements.

In parallel, clinical reference data were collected from adult CT examinations to identify representative Hounsfield Unit (HU) values for trabecular bone. Three anatomical regions predominantly composed of trabecular bone were considered: the pelvis, thoracic spine, and lumbar spine. A total of **59 pelvic, 46 ribs, and 86 lumbar** CT scans were analyzed, corresponding to **a total of 191 examinations**. ROIs were placed within these regions to extract HU values, and an average HU value was determined as representative of human trabecular bone.

To further investigate the energy dependence of the developed material, additional acquisitions were performed at 80, 100, 120, and 140 kVp. This approach enabled the evaluation of HU variation with photon energy and the assessment of the consistency of the material's radiological behavior across the diagnostic energy range.

## RESULTS

In this study, the developed bone-equivalent composite, formulated with **75% epoxy resin and 25% $TiO_2$**, was first characterized in terms of its p0068ysical properties. The material exhibited a measured mass density of **2.0 g/cm³**, while the reference density of human trabecular bone is reported to be **1.92 g/cm³**. This close agreement in density provides an initial indication of the suitability of the proposed material for simulating trabecular bone.

The energy dependence of the effective atomic number (Z_eff) for both trabecular bone and the developed epoxy–$TiO_2$ composite is presented in [Figure 1], over a broad photon energy range extending from 0.001 to 20 MeV. This representation allows a direct comparison of the radiological behavior of the two materials across the different interaction regimes. In addition, the relative deviation between the composite and trabecular bone is also illustrated to quantify the level of agreement as a function of energy.

In the low-energy range (below 30 keV), the average deviation remains relatively limited, with values typically ranging between

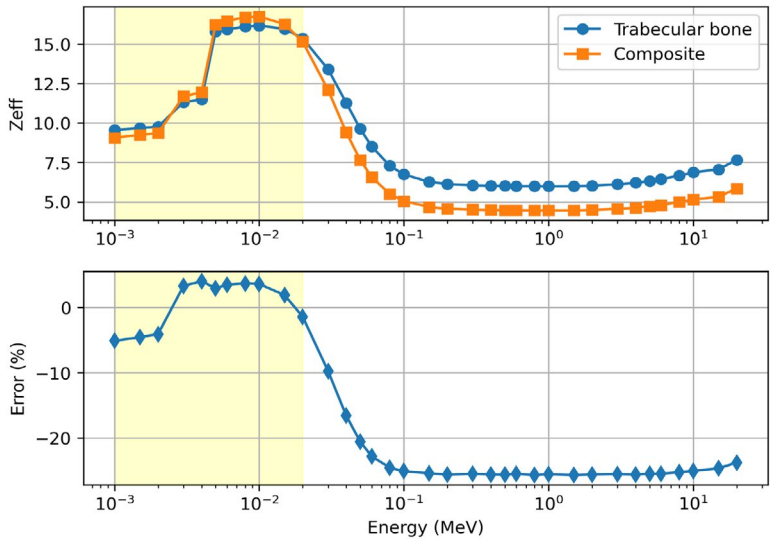


**Figure 1:** Z_eff variation and relative deviation as a function of photon energy

1**% and 5%**, indicating a good agreement between the two materials. In the intermediate energy range (40–200 keV), the discrepancy becomes more pronounced, with relative differences increasing to approximately 20**%–26%**, corresponding to the transition toward Compton-dominated interactions. Beyond 200 keV, the deviation stabilizes and remains nearly constant, with values around **19%–26%** over the high-energy range, reflecting a systematic difference between the composite and trabecular bone.

[Figure 2], reports the effective electron density (N_eff) values obtained for trabecular bone and the developed epoxy–$TiO_2$ composite across the investigated energy range. In contrast to Z_eff, which reflects the atomic composition, N_eff directly characterizes the electron population per unit volume, a parameter that governs photon scattering processes.

The Figure data include the calculated N_eff values for both materials together with the relative deviations. This presentation enables a quantitative evaluation of the proximity between the composite and trabecular bone, particularly in terms of electron density, which is a key parameter for accurately describing photon interactions in practical applications.

The results show that the effective electron density (N_eff) of the epoxy–$TiO_2$ composite remains systematically higher than that of trabecular bone across the entire investigated energy range. At low energies (< 40 keV), the discrepancy is significant, with relative differences reaching approximately 22**% to 42%**, reflecting the influence of the material composition in the photoelectric-dominated region. As the energy increases toward the diagnostic range (40–200 keV), the deviation decreases markedly, with differences typically falling within **1% to 14%**, indicating a strong convergence between the two materials. Beyond 200 keV, N_eff values for both materials exhibit a stable behavior, with a nearly constant relative difference of about 1**%–11%** over the MeV range. This trend highlights that, despite noticeable deviations at low energies, the developed composite provides a closer approximation of trabecular bone in terms of electron density under clinically relevant conditions, where Compton scattering predominates.

[Figure 3], presents the mass attenuation coefficient (μ/ρ) of trabecular bone and the developed epoxy–$TiO_2$ composite as a function of photon energy over a wide range extending from 0.01 to 15 MeV. In addition to the attenuation curves, the relative deviation between the two materials is also shown to quantify the level of agreement across the investigated energy spectrum. Unlike parameters such as Z_eff, the mass attenuation coefficient directly reflects the combined contribution of all photon interaction mechanisms, including photoelectric absorption, Compton scattering, and pair production.

The results presented in Figure X, obtained using the XCOM database based on the elemental composition of each material, show a clear energy-dependent agreement between trabecular bone and the epoxy–$TiO_2$ composite. At low energies (< 40 keV), noticeable differences are observed, with relative deviations reaching approximately **6% to 14%**, primarily due to the strong sensitivity of the photoelectric effect to atomic number and composition. As the photon energy increases into the diagnostic range (50–200 keV), the discrepancy decreases significantly, with deviations generally remaining below **2%**, indicating a strong convergence between the two materials. At higher energies (> 200 keV), the attenuation coefficients exhibit very similar behavior, with relative differences typically within **1% to 3%**, reflecting the dominance of Compton scattering and the reduced influence of elemental composition. These results confirm that, despite moderate deviations at low energies, the developed composite accurately reproduces the attenuation properties of bone over the clinically relevant energy range.

In addition to the theoretical evaluation, the radio-density of the developed composite was experimentally assessed through computed tomography by measuring the Hounsfield Unit (HU) values of the fabricated samples. The results obtained from repeated acquisitions are presented in [Figure 4], [Table 2].

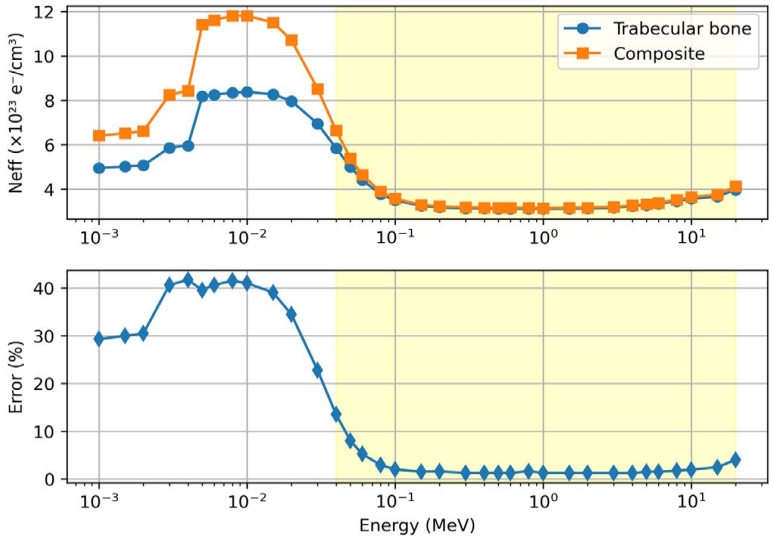


**Figure 2:** Comparison of effective electron density (N_eff) for trabecular bone and epoxy–$TiO_2$ composite across the investigated energy range

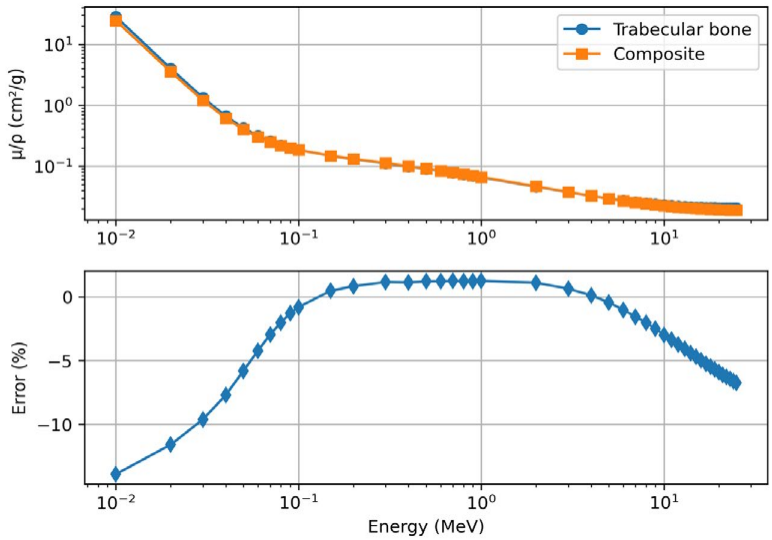


**Figure 3:** Comparison of mass attenuation coefficients (μ/ρ) for trabecular bone and epoxy–$TiO_2$ composite across the investigated energy range

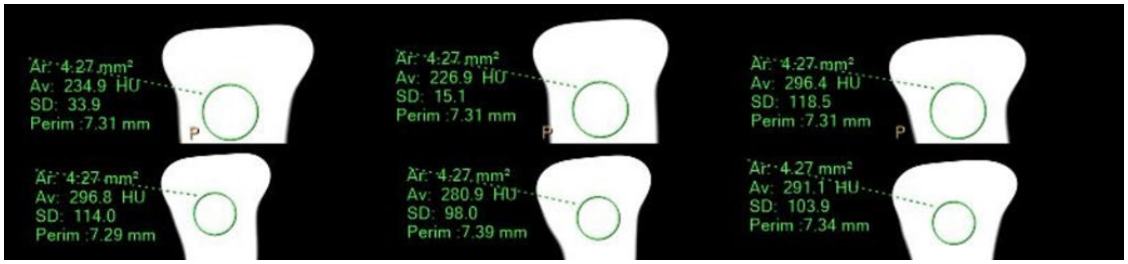


**Figure 4:** Measured Hounsfield Unit (HU) values of the fabricated epoxy–$TiO_2$ samples under clinical CT conditions

The HU measurements presented in Figure X and Table X show a moderate variability in radio-density among the fabricated samples, despite their identical composition. The measured values range from **226.9 HU to 296.8 HU**, while the reference value for human trabecular bone is **265.4 ± 3.2 HU**. This dispersion is therefore not attributed to compositional differences but rather to experimental factors such as sample positioning, local inhomogeneities, or imaging-related uncertainties. The overall mean HU value of the samples (**271.2 HU**) remains close to the reference, with a deviation of approximately **+2.2%**, indicating a good agreement with the targeted radio-density. In addition, the low coefficients of variation (CV < 1%) confirm the high reproducibility of repeated measurements for each individual sample. These results demonstrate that the developed material provides a consistent radiological response and is capable of approximating the HU range of trabecular bone under clinical CT conditions.

**Table 2:** Measured Hounsfield Unit (HU) values of the fabricated samples with corresponding statistical parameters and reference human data

| | UH | Standard deviation | Coefficient of variation % |
|---|---|---|---|
| **Sample 1** | 234.9 | 2.1 | 0.89 |
| **Sample 2** | 296.8 | 2.8 | 0.94 |
| **Sample 3** | 226.9 | 1.9 | 0.84 |
| **Sample 4** | 280.9 | 2.5 | 0.89 |
| **Sample 5** | 296.4 | 2.7 | 0.91 |
| **Sample 6** | 291.1 | 2.6 | 0.89 |
| **Pelvic trabecular bone** | 268.5 | 3.4 | - |
| **Spine trabecular bone** | 261.2 | 3.1 | - |
| **Ribs trabecular bone** | 265.4 | 3 | - |
| **Human trabecular bone** | 265.4 | 3.2 | - |

## DISCUSSION

The present study addresses the radiological characterization of an epoxy–$TiO_2$ composite designed as a trabecular bone-equivalent material over a broad photon energy spectrum extending from the kiloelectronvolt to the megaelectronvolt range. The evaluation integrates theoretical predictions derived from the XCOM database, analysis of effective electronic parameters, and experimental validation through computed tomography measurements, thereby enabling a comprehensive assessment of the material's interaction behavior.

In the low-energy range, the results indicate that the relatively small discrepancy observed in the mass attenuation coefficient (μ/ρ), typically ranging between **8% and 14%**, is directly associated with the close values of the effective atomic number (Z_eff) between the composite and trabecular bone. In this energy region, Z_eff values remain very similar, with differences on the order of **±3% to ±5%** around 10 keV, leading to comparable attenuation behavior. This relationship arises from the strong dependence of the photoelectric effect on the effective atomic number [36], which follows a highly non-linear variation with respect to Z, such that even small compositional differences can influence photon absorption [37]. However, despite significantly larger deviations observed in the effective electron density (N_eff), reaching **30% to 40%** within the same energy range, their influence on μ/ρ remains limited under these conditions [38]. Therefore, the similarity in mass attenuation coefficients between the two materials can be primarily attributed to the proximity of their Z_eff values, confirming that the photoelectric effect governs the attenuation process at low photon energies [39].

In the intermediate energy range, the attenuation behavior of the composite and trabecular bone exhibits a marked convergence, as reflected by the very small differences observed in the mass attenuation coefficient (μ/ρ), generally remaining below **2%**. For instance, at **100 keV**, μ/ρ values are **0.1855 cm²/g for trabecular bone** and **0.1840 cm²/g for the composite**, indicating an almost identical attenuation response. In contrast, the effective atomic number (Z_eff) shows a substantial divergence in this same energy range, with differences exceeding **20%**. Despite this discrepancy, the effective electron density (N_eff) values display a strong agreement, with relative differences typically within **1% to 3%**. This behavior indicates that, in this energy domain, the attenuation properties are more closely related to the electron density than to the atomic number [40,41], explaining the high level of consistency observed in μ/ρ between the two materials. These results demonstrate that, although Z_eff diverges significantly, the composite accurately reproduces the attenuation characteristics of trabecular bone within the clinically relevant diagnostic energy range.

In the high-energy region (> 200 keV), particularly within the energy range relevant to radiotherapy, the attenuation behavior of both materials reflects the contribution of high-energy photon interaction mechanisms. Above the threshold of **1.022 MeV**, **electron–positron pair production** begins to contribute to the overall attenuation process [42]. Within this regime, the mass attenuation coefficients (μ/ρ) of the composite and trabecular bone evolve in a highly similar manner, with relative differences generally remaining within **1% to 4%** across the investigated energy range. Despite the persistence of a noticeable difference in the effective atomic number (Z_eff), its influence on μ/ρ becomes less pronounced at these energies. In contrast, the effective electron density (N_eff) exhibits a stable and closely matched evolution for both materials, contributing to the observed consistency in attenuation properties [43]. The inclusion of pair production effects at higher energies further supports the overall similarity in radiological response, highlighting the capability of the developed composite to accurately reproduce the attenuation characteristics of trabecular bone under high-energy irradiation conditions relevant to radiotherapy.

The Hounsfield Unit (HU) analysis was performed as an essential experimental validation step, complementing the theoretical calculations derived from XCOM and Phy-X/PSD. Unlike these theoretical approaches, which are based on monoenergetic photon interactions, CT measurements inherently account for the **polychromatic nature of the X-ray beam**, as encountered under real clinical conditions [44]. This aspect is particularly important, as it integrates the combined effects of beam hardening and energy-dependent attenuation within a single measurable parameter [45]. The agreement observed between the measured HU values of the developed composite and the clinical reference range demonstrates that the material responds appropriately under realistic imaging conditions. Consequently, this experimental validation confirms the reliability of the developed material, reinforcing its suitability as a tissue-equivalent substitute in practical applications.

## CONCLUSION

In conclusion, the developed epoxy–$TiO_2$ composite demonstrates radiological properties comparable to trabecular bone over a wide photon energy range from keV to MeV. While differences in effective atomic number are observed, a strong agreement is achieved in mass attenuation coefficient and effective electron density within clinically relevant energy ranges. The experimental HU measurements further confirm the reliability of the material under realistic imaging conditions, accounting for the polychromatic nature of the X-ray beam. In addition, the composite provides HU values closer to clinical references compared to many existing phantoms, offering a more accurate representation of trabecular bone. Overall, the proposed material represents a reliable and cost-effective solution for the development of tissue-equivalent phantoms in both medical imaging and radiotherapy applications.

## CREDIT AUTHORSHIP CONTRIBUTION STATEMENT

- **W. Allioui:** Writing-original draft, Conceptualization.
- **Khallouqi:** Investigation, Writing-review & editing.
- **H. Sekkat:** Investigation, Writing-review & editing.
- **A. Slimani:** Investigation, Writing-review & editing.
- **A. Halimi:** Writing-review & editing, Supervision, Methodology.
- **O. El rhazouani:** Writing-review & editing, Supervision.

## DECLARATION OF COMPETING INTEREST

I hereby declare that I have no pecuniary or other personal interest, direct or indirect, in any matter that raises or may raise a conflict.

## DATA AVAILABILITY

No data was used for the research described in the article.

## ACKNOWLEDGMENTS

The authors would like to thank the Hassan 1st University Settat for the financial support.

REFERENCES


1. Purdy JA. Dose to normal tissues outside the radiation therapy patient's treated volume: a review of different radiation therapy techniques. Health Phys. 2008;95:666–676.
2. Sekkat H, El Mouden O, Khallouqi A, et al. Multi-energy gate Monte Carlo modeling and experimental validation of photon beams from an Elekta Versa HD linear accelerator in FF and FFF modes: from large to small fields. Nucl Instrum Methods Phys Res A. 2026;1088:171515.
3. Ahmed M, Melaragno LE, Nyirjesy SC, et al. Higher computed tomography (CT) scan resolution improves accuracy of patient-specific mandibular models when compared to cadaveric gold standard. J Oral Maxillofac Surg. 2023;81:1176–1185.
4. Dubec M, Price J, O'Connor J, et al. Functional image guided adaptive radiotherapy (FIG-ART) in PBT H+N treatment planning for changes in hypoxia using oxygen-enhanced MRI imaging. Int J Particle Ther. 2024;12:100190.
5. De Crevoisier R, Lafond C, Bessières I, et al. Image-guided radiotherapy: from prepositioning to treatment delivery. Cancer Radiother. 2026;30:104804.
6. McGrath S, Kestin L, Dilworth J, et al. Adaptive image guided radiotherapy (IGRT) eliminates the risk of geometric miss due to rectal distention in prostate cancer treatment planning: biochemical and clinical evidence of efficacy. Int J Radiat Oncol Biol Phys. 2008;72(Suppl):S324.
7. Sekkat H, Khallouqi A, Bannan A, et al. Validation of a cost-effective heterogeneous pediatric head phantom for CT-based HU-density calibration in radiotherapy treatment planning: a dosimetric evaluation in pediatric brain tumor cases. Radiat Phys Chem. 2025;237:113068.
8. Cabahug JPC, Tatu-Qassim SS, Ballesteros LM, et al. Characterization and evaluation of tissue-equivalent materials for heterogeneous mouse model phantoms in radiobiology experiments. Radiat Phys Chem. 2025;237:113034.
9. Podgorsak EB. Interactions of photons with matter. In: Radiation Physics for Medical Physicists. Springer; 2016.
10. Manjunatha HC, Rudraswamy B. Study of effective atomic number and electron density for tissues from human organs in the energy range of 1 keV–100 GeV. Health Phys. 2013;104:158.
11. Pratt RH, Ron A, Tseng HK. Atomic photoelectric effect above 10 keV. Rev Mod Phys. 1973;45:273–325.
12. Hizó J. A calculation method of material equivalence relating to photoelectric interactions. 1982.
13. Springer Nature. Compton effect.
14. Modélisation et correction de l'effet Compton dans la reconstruction d'images tomoscintigraphiques. Theses.fr record. 1997.
15. Tsiamas P, Brown SL, Chetty IJ, et al. Dosimetric evaluation and beam characterization of pair production enhanced radiotherapy (PPER) with the use of organometallics. Phys Med Biol. 2019;64:075014.
16. Glick SJ, Ikejimba LC. Advances in digital and physical anthropomorphic breast phantoms for X-ray imaging. Med Phys. 2018;45.
17. Followill DS, Evans DR, Cherry C, et al. Design, development, and implementation of the Radiological Physics Center's pelvis and thorax anthropomorphic QA phantoms. Med Phys. 2007;34:2070–2076.
18. Goodsitt MM, Christodoulou EG, Larson SC, et al. Assessment of calibration methods for estimating bone mineral densities in trauma patients with quantitative CT: an anthropomorphic phantom study. Acad Radiol. 2001;8:822–834.
19. Tino RB, Yeo AU, Brandt M, et al. A customizable anthropomorphic phantom for dosimetric verification of 3D-printed lung, tissue, and bone density materials. Med Phys. 2022;49:52–69.
20. Breslin T, Paino J, Wegner M, et al. A novel anthropomorphic phantom composed of tissue-equivalent materials for experimental radiotherapy. Biomimetics. 2023;8:230.
21. Winslow JF, Hyer DE, Fisher RF, et al. Construction of anthropomorphic phantoms for use in dosimetry studies. J Appl Clin Med Phys. 2009;10:195–204.
22. Molineu A, Followill DS, Balter PA, et al. Design and implementation of an anthropomorphic QA phantom for IMRT for the Radiation Therapy Oncology Group. Int J Radiat Oncol Biol Phys. 2005;63:577–583.
23. Tajik M, Akhlaqi MM, Gholami S. Advances in anthropomorphic thorax phantoms for radiotherapy: a review. Biomed Phys Eng Express. 2022;8:052001.
24. Colvill E, Krieger M, Bosshard P, et al. Anthropomorphic phantom for deformable lung and liver CT and MR imaging for radiotherapy. Phys Med Biol. 2020;65:07NT02.
25. Cavaliere C, Baldi D, Brancato V, et al. A customized anthropomorphic 3D-printed phantom to reproducibility assessment in computed tomography. Front Oncol. 2023;13.
26. Bergot C, Bocquet JP. Étude systématique, en fonction de l'âge, de l'os spongieux et de l'os cortical de l'humérus et du fémur. 1976.
27. Chappard D, Baslé MF, Legrand E, et al. Trabecular bone microarchitecture: a review. Morphologie. 2008;92:162–170.
28. Customizable anthropomorphic phantom for dosimetric verification of 3D-printed lung tissue bone density materials.
29. ICRU. Tissue substitutes in radiation dosimetry and measurement. ICRU Report 44. 1989.
30. Turner AC, Zhang D, Khatonabadi M, et al. Patient size-corrected, scanner-independent organ dose estimates for abdominal CT exams. Med Phys. 2011;38:820–829.
31. Valentin J. Basic anatomical and physiological data for use in radiological protection: reference values (ICRP Publication 89). Ann ICRP. 2002;32:1–277.
32. Aziz HA, Jasim WN. Theoretical analysis of the X-ray mass absorption coefficient produced by the photoelectric effect and comparison of the accuracy of a computational model of NiO and SiC. Mod J Health Appl Sci. 2025;2:86–95.
33. Bouchard-Gilanton V. Modélisation et correction de l'effet Compton dans la reconstruction d'images tomoscintigraphiques. Thesis. 1997.
34. Al-Hadeethi Y, Sayyed MI. Evaluation of gamma ray shielding characteristics of CaF2–BaO–P2O5 glass system using PHY-X/PSD program. Prog Nucl Energy. 2020;126:103397.
35. Elbashir BO, Dong MG, Sayyed MI, et al. Comparison of Monte Carlo simulation of gamma ray attenuation coefficients of amino acids with XCOM program and experimental data. Results Phys. 2018;9:6–11.
36. Cesareo R, Hanson AL, Gigante GE, et al. Interaction of keV photons with matter and new applications. Phys Rep. 1992;213:117–178.
37. Locher GL. The compound photoelectric effect of X-rays in light elements. Phys Rev. 1932;40:484–495.
38. Fournet G. Étude théorique et expérimentale de la diffusion des rayons X par les ensembles denses de particules. 1951.
39. Huy BN, Van Dung P, Tinh HT, et al. Photon energy estimation in diagnostic radiology using OSL dosimeters: experimental validation and Monte Carlo simulations. Radiat Meas. 2025;180:107342.
40. Evans RD. Compton effect. In: Flügge S, ed. 1958:218–298.
41. Moscovici J, Loupias G, Rabii S, et al. Compton profiles and electronic density in C60. EPL. 1995;31:87.

42. Physique fondamentale des rayonnements ionisants — radiobiologie — radioprotection. ScienceDirect chapter.

43. Knöös T, Nilsson M, Ahlgren L. A method for conversion of Hounsfield number to electron density and prediction of macroscopic pair production cross-sections. Radiother Oncol. 1986;5:337–345.

44. Enhancement of X-ray computerized tomographic images considering the polychromatic nature of X-rays. ProQuest record.

45. Menvielle N, Goussard Y, Orban D, et al. Reduction of beam-hardening artifacts in X-ray CT. IEEE EMBC. 2005:1865–1868.